Featured Article

Human stem cell–derived monocytes and microglia-like cells reveal impaired amyloid plaque clearance upon heterozygous or homozygous loss of TREM2

Christel Claes[a,b], Johanna Van Den Daele[a,b], Ruben Boon[a], Sarah Schouteden[a], Alessio Colombo[c], Laura Sebastian Monasor[c], Mark Fiers[b], Laura Ordovás[a], FatemehArefeh Nami[a], Bernd Bohrmann[d], Sabina Tahirovic[c], Bart De Strooper[b], Catherine M. Verfaillie[a,*]

[a]Department of Development and Regeneration, Stem Cell Biology and Embryology, KU Leuven Stem Cell Institute, Leuven, Belgium
[b]Laboratory for the Research of Neurodegenerative Diseases, VIB-KU Leuven Center for Brain & Disease Research, Leuven, Belgium
[c]German Center for Neurodegenerative Diseases (DZNE), Munich, Germany
[d]Roche Pharmaceutical Research and Early Development NORD Discovery & Translational Area, Roche Innovation Center Basel, Basel, Switzerland

Abstract

Introduction: Murine microglia expressing the Alzheimer's disease–linked $TREM2^{R47H}$ mutation display variable decrease in phagocytosis, while impaired phagocytosis is reported following loss of TREM2. However, no data exist on $TREM2^{+/R47H}$ human microglia. Therefore, we created human pluripotent stem cell (hPSC) monocytes and transdifferentiated microglia-like cells (tMGs) to examine the effect of the $TREM2^{+/R47H}$ mutation and loss of $TREM2$ on phagocytosis.

Methods: We generated isogenic $TREM2^{+/R47H}$, $TREM2^{+/-}$, and $TREM2^{-/-}$ hPSCs using CRISPR/Cas9. Following differentiation to monocytes and tMGs, we studied the uptake of *Escherichia coli* fragments and analyzed amyloid plaque clearance from cryosections of $APP/PS1^{+/-}$ mouse brains.

Results: We demonstrated that tMGs resemble cultured human microglia. $TREM2^{+/-}$ and $TREM2^{-/-}$ hPSC monocytes and tMGs phagocytosed significantly less *E. coli* fragments and cleared less amyloid plaques than wild-type hPSC progeny, with no difference for $TREM2^{+/R47H}$ progeny.

Discussion: *In vitro* phagocytosis of hPSC monocytes and tMGs was not affected by the $TREM2^{+/R47H}$ mutation but was significantly impaired in $TREM2^{+/-}$ and $TREM2^{-/-}$ progeny.
© 2018 The Authors. Published by Elsevier Inc. on behalf of the Alzheimer's Association. This is an open access article under the CC BY-NC-ND license (http://creativecommons.org/licenses/by-nc-nd/4.0/).

Keywords: Alzheimer's disease; TREM2; Human pluripotent stem cells; Microglia; Monocytes; Phagocytosis; Human amyloid plaques

1. Introduction

Abnormal amyloid processing and plaque formation in patients with familial Alzheimer's disease (AD) are caused by mutations in the *APP* or *PSEN1/2* gene that directly affect the production of amyloid [1–3]. However, late-onset AD (LOAD) and Nasu-Hakola disease (NHD) patients, who lack these mutations, also present with amyloid pathology and dementia [4–6]. Genome-wide association studies revealed that mutations in immune genes, including *TREM2*, are risk factors for patients with LOAD [3–5,7,8], while homozygous loss of cell surface–expressed TREM2 on microglia causes NHD [9,10]. Thus, microglia dysfunction not only occurs in response to neurodegeneration but may also be sufficient to induce amyloid pathology and contributes to disease progression [11–13].

TREM2 is expressed intracellular and on the membrane of myeloid cells, in particular microglia [14–17]. Single-nucleotide polymorphisms (SNPs) in *TREM2* significantly

*Corresponding author. Tel.: +3216 372654; Fax: +3216 330294.
E-mail address: catherine.verfaillie@kuleuven.be

increase the risk of developing multiple neurological disorders. In individuals with a heterozygous *TREM2 R47H* mutation (*TREM2$^{+/R47H}$*), there is a 3-fold increased risk for LOAD, approximating the risk imposed by apolipoprotein E4 (APOE ε4) [4,5,18,19]. Although *TREM2* appears to be crucial for microglial activation [20], and is required for a broad range of microglial responses to neurodegeneration (e.g., proliferation, migration, phagocytosis, inflammatory response, survival, clustering, cellular energetic and biosynthetic metabolism) [21–28], it remains unclear how *TREM2* mutations cause AD pathology. One possibility would be that certain *TREM2* mutations directly affect amyloid clearance. The *R47H* mutation was shown to not impair amyloid plaque load in mice [27] but to reduce amyloid compaction, which was also observed upon TREM2 deficiency [23]. Nevertheless, murine *in vivo* studies revealed variable results on plaque load following loss of TREM2, which appeared to be time dependent [22]. *In vitro*, decreased phagocytosis of several ligands (e.g., latex beads, pHrodo-linked *Escherichia coli* fragments, amyloid β$_{1–42}$ fragments [29], neurons [30,31], and reduced amyloid plaque clearance [32]) has consistently been demonstrated in TREM2-deficient mouse macrophages, microglia, and HEK cell lines. However, Brownjohn et al. recently observed no defect in *E. coli* uptake in microglia-like cells derived from human pluripotent stem cells (hPSCs) carrying mutations that cause a decrease/absence of mature TREM2 membrane expression [33]. The effect of the *R47H* mutation on *in vitro* phagocytosis has solely been studied in transduced HEK cells and mouse microglia with inconsistent results: *R47H* transduced HEK cells displayed a reduced uptake of latex beads, and amyloid β$_{1–42}$, but not pHrodo-linked *E. coli* fragments [29]. In addition, the degree of reduced latex bead uptake differed between *R47H* mutant transduced HEK cells [29] and microglia [34], and amyloid plaque removal has so far not been assessed.

To examine if the AD-associated heterozygous *R47H* mutation, or heterozygous or homozygous loss of *TREM2*, can directly impair phagocytosis by human microglia, we generated hPSC-derived *TREM2$^{+/R47H}$*, *TREM2$^{+/-}$*, and *TREM2$^{-/-}$* monocytes and microglia-like cells and performed two independent phagocytosis assays including an *ex vivo* human amyloid plaque clearance assay.

2. Methods

2.1. Human PSC differentiation to monocytes and transdifferentiated microglia-like cells

Monocytes were differentiated according to the protocol published by Yanagimachi et al. [35]. On days 17, 21, 25, 28, and 32, nonadherent cells were harvested and monocytes selected using CD14-labeled magnetic beads (Miltenyi), according to the company's specifications. Monocytes were used for further analysis on the day of collection. To transdifferentiate monocytes to microglia-like cells (transdifferentiated microglia-like cells [tMGs]), a minimum of 500,000 freshly harvested monocytes were plated per well of a 6-well plate (Corning) in the microglia differentiation medium (Neurobasal medium, N2, B27, lactic acid, sodium pyruvate, glutamax, biotin, ascorbic acid, NaCl, Albumax I, and Pen/Strep.) supplemented with 10 ng/mL of IL34 and M-CSF, resembling the microglia medium described by Muffat et al. [36]. The medium was changed every day. The yield of monocytes per 6-well plate (5–10 colonies/well) varied between 5×10^5 and 1×10^6, and an equal number of adherent tMGs were obtained.

2.2. Genome engineering

To create *TREM2$^{+/-}$* and *TREM2$^{+/R47H}$* from H9 wild-type (WT) human embryonic stem cells (Supplementary Methods 1.1. and 1.3.), CRISPR/Cas9 nickases and two guide RNAs (gRNA A and B) (Supplementary Table 1) that target exon 2 of *TREM2* nearby the location of *R47H* (*G>A*) and a genomic *TTAA* were purchased from Addgene. A donor plasmid was made comprising homology arm 1 (HA1) of *TREM2* (with the *R47H* mutation), a selection cassette (CAGG promoter, HYG/TK, green fluorescent protein) and HA2 of *TREM2* exon 2. To create *TREM2$^{-/-}$* hPSCs, a CRISPR/Cas9, gRNA B, and the same donor plasmid were used. To create *TREM2$^{+/R47H}$* hPSCs, 2×10^6 single cells of the heterozygously targeted clone were nucleofected with 4 μg of piggyBac (PB) transposase plasmid and negative selection with fialuridine, also known as 1-(2-deoxy-2-fluoro-1-D-arabinofuranosyl)-5-iodouracil (FIAU) (1:8000–1:2500; 0.5 mM in water), was applied to select for cells wherein the selection cassette was removed. Of note, the H9 WT line from which the *TREM2$^{+/R47H}$*, *TREM2$^{+/-}$*, and *TREM2$^{-/-}$* lines were created carries an APOE ε3/ε4 genotype [37].

2.3. Ex vivo amyloid plaque clearance

The *ex vivo* amyloid plaque clearance assay was performed as described by Xiang et al., 2016 [32,38]; 10-μm-thick cryosections from 6-month-old *APP/PS1$^{+/-}$* mouse brains [39] were collected onto poly-L-lysine-coated glass coverslips, dried at room temperature for 1 h, followed by incubation with 5 μg/mL mAb11 antibody in phosphate-buffered saline (PBS) for 1 h at 37°C. Human PSC monocytes were seeded at 3×10^5 and tMGs at 2×10^5 per well in 12-well plates and incubated at 37°C with 5% CO$_2$ for 16 h/24 h in either a monocyte medium (day 13 composition) or microglia differentiation medium with IL34 and M-CSF for tMGs. *TREM2* WT (wild-type), *TREM2$^{+/R47H}$*, *TREM2$^{+/-}$*, or *TREM2$^{-/-}$* cells were plated on consecutively cut cryosections to ensure comparable amyloid plaque load. We also included *APP/PS1$^{+/-}$* cryosections without hPSC progeny as a control. After incubation, coverslips were fixed with 4% paraformaldehyde for 15 minutes, permeabilized using 0.1% Triton in 1× PBS; blocked for 1 h
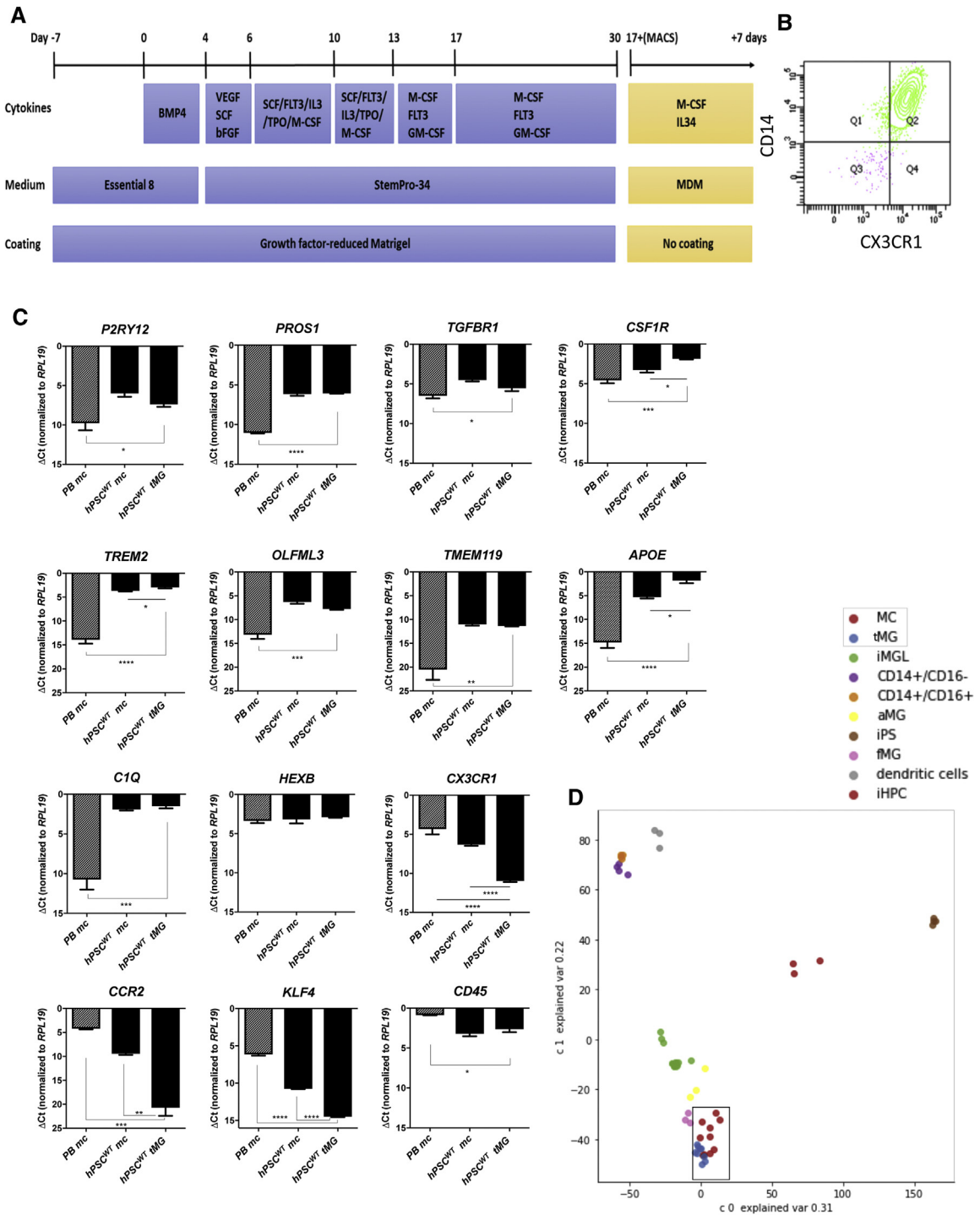
Fig. 1. Differentiation of monocytes (mc) and tMG from *TREM2 WT, TREM2*$^{+/R47H}$, *TREM2*$^{+/-}$, *and TREM2*$^{-/-}$ hPSC lines. (A) The protocol used to differentiate hPSC-derived mc (based on Yanagimachi et al., 2013) and subsequent differentiation of MACS sorted CD14$^+$ cells to tMG, based on medium adapted from Muffat et al., 2016 (MDM). (B) The representative flow cytometry plot of CD14-MACS purified mc for CD14 and CX3CR1; MACS was performed 5 times between days 17 and 32. (C) qRT-PCR for microglial and monocyte genes of PB mc, hPSC mc, and hPSC tMG (ΔCt normalized to *RPL19*). (D) The principal component analysis plot of RNAseq data (hPSC-monocytes [MC] and tMG, marked) merged with the data set from the Abud et al., 2017, including their samples from iMGLs (hPSC-derived microglia-like cells), CD14$^+$ peripheral blood monocytes, aMG (cultured human primary adult microglia), iPS (human-induced pluripotent stem cells), fMG (cultured human primary fetal microglia), dendritic cells, and iHPC (stem cell-derived hematopoietic progenitors). All qRT-PCR data represent N = 3, means with SEM, and *P* values by unpaired *t*-test; *$P \leq .05$; **$P < .005$; ***$P < .001$; ****$P < .0001$. Abbreviations: iMGL, induced microglia-like cells; hPSC, human pluripotent stem cell; MDM, microglia differentiation medium; tMG, transdifferentiated microglia-like cells; WT, wild-type.
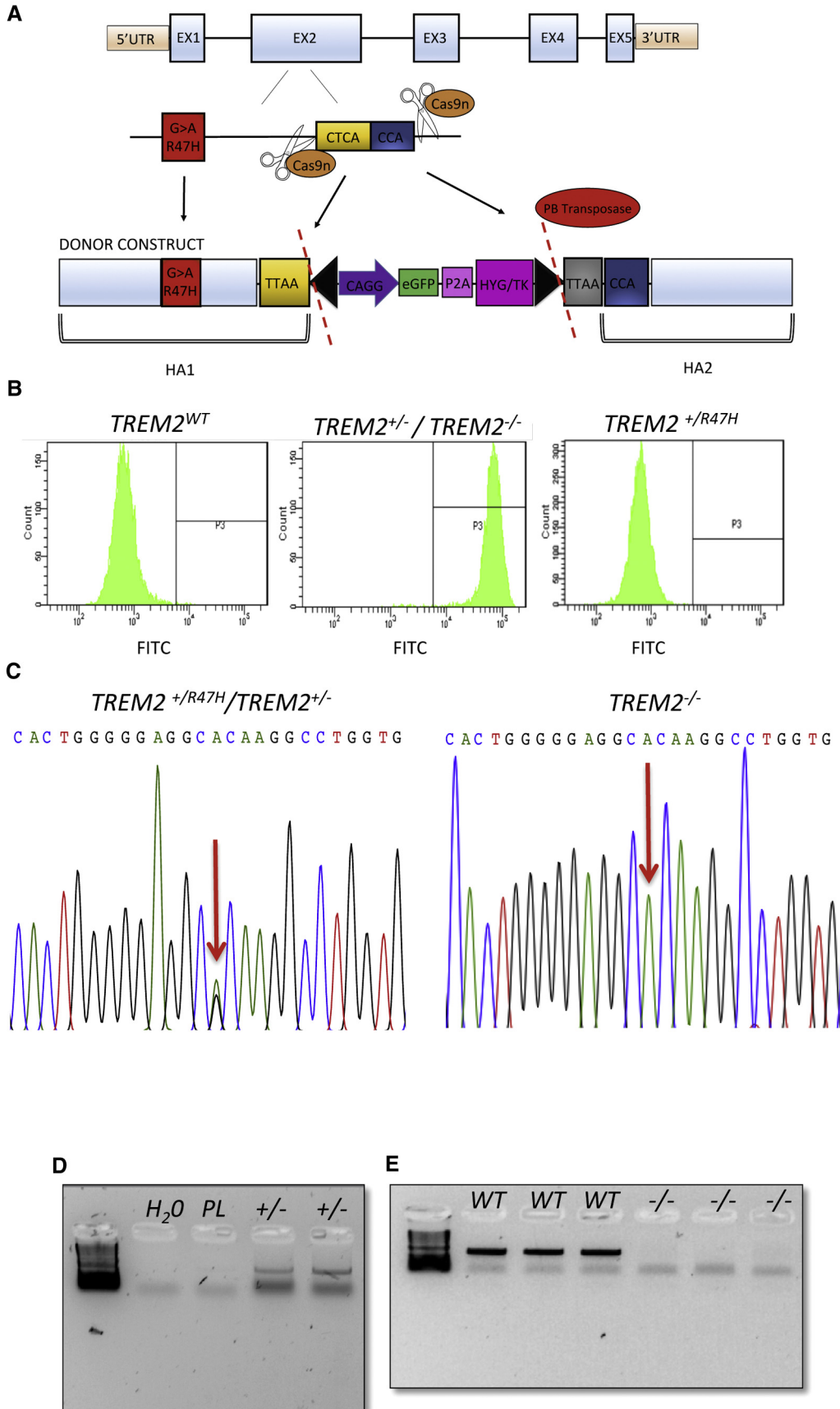
with 2% fetal calf serum, 2% bovine serum albumin, and 0.2% fish gelatin in $1\times$ PBS; and stained with an anti-LAMP1 antibody (Sigma Aldrich; Rb, 1:100) to visualize lysosomes in monocytes and tMGs, or 3552 amyloid β antibody (1:5000) ([40]; provided by Harald Steiner LMU, Munich) for 1 h at room temperature. Secondary staining included thiazine red to visualize amyloid plaques (2 μg/ml; Sigma), goat anti-rabbit Alexa Fluor-488 (1:500; Thermo Fisher Scientific), and Hoechst (1:2000) for 45 minutes at room temperature. After washing with PBS and water, coverslips were placed in mounting medium on glass slides. Three to four images of cortical areas were acquired on an epifluorescence microscope (Zeiss Axio Imager A2) equipped with AxioCam MRm using AxioVision software package and on a Leica SP5 confocal microscope. The number and area of the thiazine red signals (555) were analyzed by ImageJ (NIH). The number and area of plaques from sections incubated with $TREM2^{+/R47H}$, $TREM2^{+/-}$, or $TREM2^{-/-}$ tMGs or monocytes were compared with $TREM2$ WT cells. Results were plotted and analyzed using GraphPad Prism 6 software. Ethical approval for this work was obtained under project number P026/2016.

2.4. Additional methods

Other methods used in this study can be found in the Supplementary Methods online.

2.5. Statistical methods

Data represent minimum of two to three independent differentiations with technical replicates, means with SEM, and P values by unpaired t-test: $*P \leq .05$; $**P < .005$; $***P < .001$; and $****P < .0001$.

3. Results

3.1. Differentiation to monocytes and tMGs

Monocytes were generated using the Yanagimachi protocol [35] (Fig. 1A and Supplementary Fig. 1A). From day 17 onward, $CD14^+$ monocytes were isolated from the medium by magnetic-activated cell sorting (MACS). MACS-isolated monocytes were nearly 100% CX3CR1 and CD14 positive (Fig. 1B). Once transdifferentiated to tMGs, cells became

adherent and stained nearly 100% TMEM119 and IBA1 positive (Supplementary Fig. 1B).

Transdifferentiated microglia-like cells expressed significantly higher levels of microglial gene transcripts (*P2RY12, PROS1, TGFBR1, OLFML3, C1Q, CSF1R, TMEM119, APOE,* and *TREM2* [Fig. 1C]) compared with human peripheral blood (PB) monocytes, measured by qRT-PCR. Transcripts for *HEXB* were already highly expressed in PB monocytes, and *CX3CR1* transcripts were lower in tMGs than PB monocytes (Fig. 1C). Compared with hPSC monocytes, typical microglial transcripts were not higher expressed in tMGs, except for *TREM2, APOE,* and *CSF1R* (Fig. 1C), whereas transcript levels of *CD45,* a marker of definitive bone marrow–derived macrophages [41], were lower in both hPSC monocytes and tMGs than PB monocytes (Fig. 1C). However, tMGs expressed significantly lower levels of the monocyte gene *CCR2* and the monocyte-specific transcription factor *KLF4* [41] (Fig. 1C) than hPSC monocytes and PB monocytes. Thus, this limited transcriptional analysis suggested that hPSC-derived tMGs resemble microglia. Surprisingly, monocytes derived via the Yanagimachi protocol from hPSCs [35] were more similar to tMGs than PB monocytes (Fig. 1C). This was confirmed by genome-wide RNA sequencing (RNAseq) studies, where we compared tMGs and hPSC monocytes generated in this study with the RNAseq data from Abud et al. [41]. Principal component analysis of both data sets demonstrated that tMGs and hPSC monocytes generated from our study clustered together with *in vitro* cultured human fetal and adult human microglia, and with hPSC-induced microglia-like cells, but not with $CD14^+$ PB monocytes (Fig. 1D). This was further confirmed by the similarity in the gene expression patterns observed for the normalized log1p CPM (counts per million) for a set of genes of the two RNAseq studies (Supplementary Fig. 1C). Thus, hPSC monocytes derived using the Yanagimachi protocol differ from PB monocytes, which we hypothesize is caused by *in vitro* culture. Indeed, *in vitro* culture of PB monocytes for 48 h in the culture medium used to create monocytes from hPSCs increased expression of a set of microglial genes (Supplementary Fig. 1D).

Thus, we do not only provide evidence that the tMGs described in the present study resemble microglia-like cells generated in other published studies, and cultured human

Fig. 2. Genome engineering of isogenic $TREM2^{+/R47H}$, $TREM2^{+/-}$, and $TREM2^{-/-}$ hPSC lines. (A) Genomic targeting of exon 2 of the human $TREM2$ gene by means of CRISPR/Cas9 nickases to create $TREM2^{+/R47H}$ and $TREM2^{+/-}$ hPSCs; to create $TREM2^{-/-}$ CRISPR/Cas9, gRNA B (Supplementary Table 1) and the same donor construct were used to result in homozygous insertion of the selection cassette. (B) The representative flow cytometry plot for GFP (emission in the FITC field) after positive selection with hygromycin—left to right: H9 WT isogenic line 0 % $FITC^+$, $TREM2^{+/-}$ line (heterozygous) or $TREM2^{-/-}$ line (homozygous) 100 % $FITC^+$, and after subsequent removal of the selection cassette from the $TREM2^{+/-}$ hPSC line by piggyBac transposase and negative selection (FIAU), $TREM2^{+/R47H}$ hPSCs (0 % $FITC^+$). (C) Sequencing of HA1 demonstrating presence of the *R47H* mutation *(G>A)* in one allele of $TREM2$ for $TREM2^{+/R47H}$ and $TREM2^{+/-}$ and both alleles for $TREM2^{-/-}$; note that without removal of the selection cassette by piggyBac transposase the targeted allele(s) encompassing this mutation will not be transcribed. (D) Cell PCR of selected clones demonstrated heterozygous targeting and (E) homozygous targeting of $TREM2$, as a control WT gDNA (H9 isogenic control), donor construct alone (PL), or water was used in the appropriate buffer. Abbreviations: GFP, green fluorescent protein; hPSC, human pluripotent stem cell; WT, wild-type.

primary microglia, but we also demonstrate that hPSC monocytes more closely resemble microglia-like cells than primary PB monocytes, likely caused by the *in vitro* culture of hPSC monocytes.

3.2. Genome engineering of TREM2 mutant hPSC lines

To assess the role of *TREM2* mutations or loss of *TREM2* in human microglia, we used CRISPR/Cas9-mediated genome engineering. We inserted by homologous recombination a donor construct, encompassing the *R47H* SNP, a 6-kB hygromycin/thymidine kinase selection cassette between two piggyBac inverted repeat sequences, and a silent mutation (*CTCA>TTAA*), in exon 2 of *TREM2* (Fig. 2A). Inducing a silent *TTAA* mutation within 300 bp of the wanted *R47H* SNP was needed to enable piggyBac excision of the selection cassette after targeting [42] (Fig. 2A). Insertion of the 6-kB cassette in exon 2, in either one allele (CRISPR/Cas9 nickases + gRNA A and B) [43] or both alleles (CRISPR/Cas9 + gRNA B), interferes with its transcription and resulted in a $TREM2^{+/-}$ and $TREM2^{-/-}$ hPSC line (Supplementary Table 1). Following excision of the selection cassette by piggyBac transposase [42], the *R47H* heterozygous line ($TREM2^{+/R47H}$) was created from the $TREM2^{+/-}$ line (Fig. 2A). Successful targeting and subsequent removal of the selection cassette from the $TREM2^{+/-}$ line to create the $TREM2^{+/R47H}$ mutant line was confirmed by presence and absence of green fluorescent protein expression (emission in the FITC field) before and after piggyBac excision (Fig. 2B). Quality control studies consisted of sequencing of *TREM2* exon 2 (*G>A, R47H*) (Fig. 2C; Supplementary Table 2), PCR genotyping (5′ junction assay [JA], 5′ random integration [RI], and cell PCR) (Fig. 2D, E; Supplementary Fig. 2A, B; Supplementary Table 2), sequencing of the top 3 predicted off-target sites of each gRNA (Supplementary Fig. 2C, D), array comparative genome hybridization (Supplementary Fig. 2E), SNP profiling for cell identity, and pluripotency assays (immunohistochemistry and score cards) (Supplementary Fig. 2F).

3.3. Characterization of hPSC monocytes and tMGs derived from TREM2 WT, $TREM2^{+/R47H}$, $TREM2^{+/-}$, and $TREM2^{-/-}$ hPSCs

Quantitative RT-PCR analysis demonstrated that heterozygous or homozygous cassette integration in exon 2 of *TREM2* resulted in a reduction of *TREM2* mRNA in $TREM2^{+/-}$ compared with WT progeny (reduction of +/− 3 ΔCt), with a greater reduction in $TREM2^{-/-}$ compared with $TREM2^{+/-}$ progeny (reduction of +/− 5 ΔCt) (Fig. 3A).

Following differentiation of the different *TREM2* lines to hPSC monocytes and tMGs, we observed a similar increased expression of monocyte-related genes in all *TREM2* hPSC monocytes (*CD14, CD45, CCR2, DAP12,* and *CX3CR1*; Supplementary Table 3) and reduced *OCT4* expression relative to WT hPSCs (Fig. 3B). Moreover, expression of a panel of microglia markers (Supplementary Table 3) was highly similar in the different *TREM2* tMG variants relative to WT tMGs (Fig. 3C).

We next compared the transcriptome of WT and $TREM2^{-/-}$ tMGs by RNA sequencing. Supplementary Table 4 shows the top affected functions that were upregulated or downregulated in $TREM2^{-/-}$ tMGs compared with WT tMGs. The highest downregulated functions included extracellular matrix structure and transmembrane transporter activity. The highest upregulated functions in $TREM2^{-/-}$ tMGs included receptor-ligand activity, receptor-regulator activity, calcium ion binding, and cytokine activity (Supplementary Table 4 and 5).

3.4. $TREM2^{+/-}$ and $TREM2^{-/-}$, but not $TREM2^{+/R47H}$ monocytes and tMGs, phagocytosed significantly less pHrodo-linked E. coli fragments

We assessed the ability of WT, $TREM2^{+/R47H}$, $TREM2^{+/-}$ and $TREM2^{-/-}$ monocytes and tMGs to phagocytose pHrodo-linked *E. coli* fragments using 100,000 cells and analyzed after 10 minutes of incubation. Compared with WT cells, $TREM2^{+/-}$ and $TREM2^{-/-}$ monocytes and tMGs phagocytosed significantly less *E. coli* fragments (Fig. 4A, B; Supplementary Fig. 3). In contrast, the $TREM2^{+/R47H}$ mutation in tMGs did not affect phagocytosis of *E. coli* (Fig. 4B) and decreased phagocytosis by hPSC monocytes by only 4% compared with WT cells (Fig. 4A, Supplementary Fig. 3).

3.5. Amyloid plaque clearance from $APP/PS1^{+/-}$ cryosections was reduced for $TREM2^{+/-}$ and $TREM2^{-/-}$, but not $TREM2^{+/R47H}$ monocytes and tMGs

We also plated WT, $TREM2^{+/R47H}$, $TREM2^{+/-}$, and $TREM2^{-/-}$ monocytes and tMGs onto cryosections from 6-month-old $APP/PS1^{+/-}$ mouse brains, containing amyloid plaques [39]. Xiang et al. [32] demonstrated that preincubation of $APP/PS1^{+/-}$ cryosections with mAb11 antibody, a murine IgG2a antibody with similar amyloid binding properties as the clinically used anti-Aβ antibody Gantenerumab [44,45], triggers amyloid plaque clearance by exogenously added mouse microglia. Similarly, hPSC monocytes robustly removed amyloid plaques after 48 h (Supplementary Fig. 4A), as shown by reduced staining of Aβ plaques using thiazine red and anti-amyloid β antibody (3552 Ab-green), which was not observed in the absence of mAb11 (Supplementary Fig. 4A).

We next determined the kinetics of amyloid removal by staining brain cryosections with thiazine red (amyloid plaque cores) and 3552 antibody (amyloid β antibody) from 7 h to 72 h after incubation of the hPSC monocytes on the $APP/PS1^{+/-}$ cryosections. Twenty-four hours was chosen
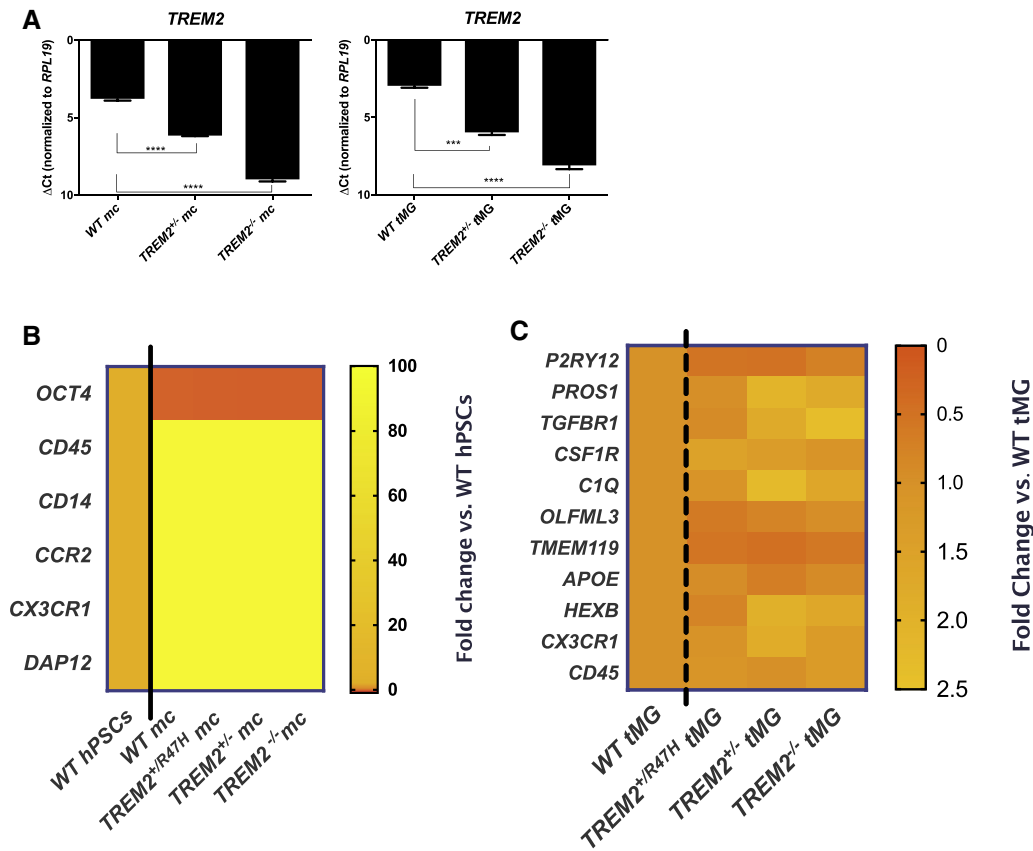
Fig. 3. TREM2 expression and characterization of isogenic *TREM2*[+/R47H], *TREM2*^{+/−}, *and TREM2*^{−/−} hPSC progeny. (A) qRT-PCR analysis of *TREM2* transcript levels in *TREM2*^{+/−} and *TREM2*^{−/−} monocytes and tMG. (B) Heatmap representation of qRT-PCR data for monocyte transcripts and *OCT4*, in mc derived from the different cell lines ($2^{-(\Delta Ct\ target\ -\ \Delta Ct\ control)}$), relative to the calibrator (control) WT hPSCs; (ΔCt normalized to *RPL19*). (C) Heatmap representation of qRT-PCR data for microglial transcripts in tMG derived from the different cell lines ($2^{-(\Delta Ct\ target\ -\ \Delta Ct\ control)}$, relative to the calibrator (control) WT tMG; (ΔCt normalized to *RPL19*). (B, C) Higher fold expression (>1) compared to the control (=1) is highlighted in a lighter color; lower fold expression (<1) compared to the control (=1) is highlighted in a darker color. All data represent N = 3, means with SEM, and *P* values by unpaired *t*-test; *$P \leq .05$; **$P < .005$; ***$P < .001$; ****$P < .0001$. Abbreviations: hPSC, human pluripotent stem cell; WT, wild-type.
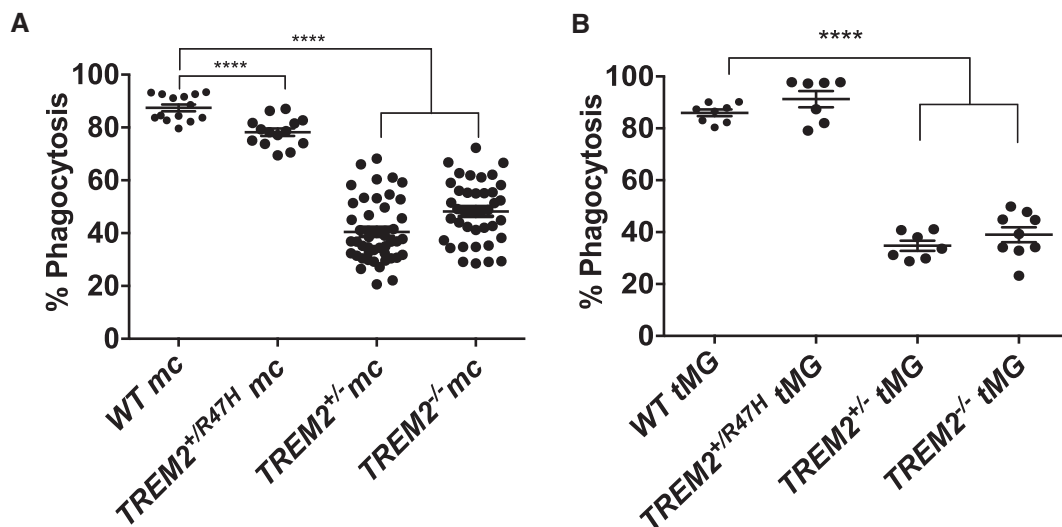

Fig. 4. Uptake of *pHrodo-linked E. coli* fragments by *TREM2 WT*, *TREM2*[+/R47H], *TREM2*^{+/−}, and *TREM2*^{−/−} mc, and tMG. (A, B) Uptake of *pHrodo*-labeled *E. coli* fragments by *TREM2 WT*, *TREM2*[+/R47H], *TREM2*^{+/−}, and *TREM2*^{−/−} monocytes (mc) (A) and tMG (B); for each cell line, N ≥ 3 differentiations. Data represent means with SEM and *P* values by unpaired *t*-test; ****$P < .0001$. Abbreviations: tMG, transdifferentiated microglia-like cells; WT, wild-type.
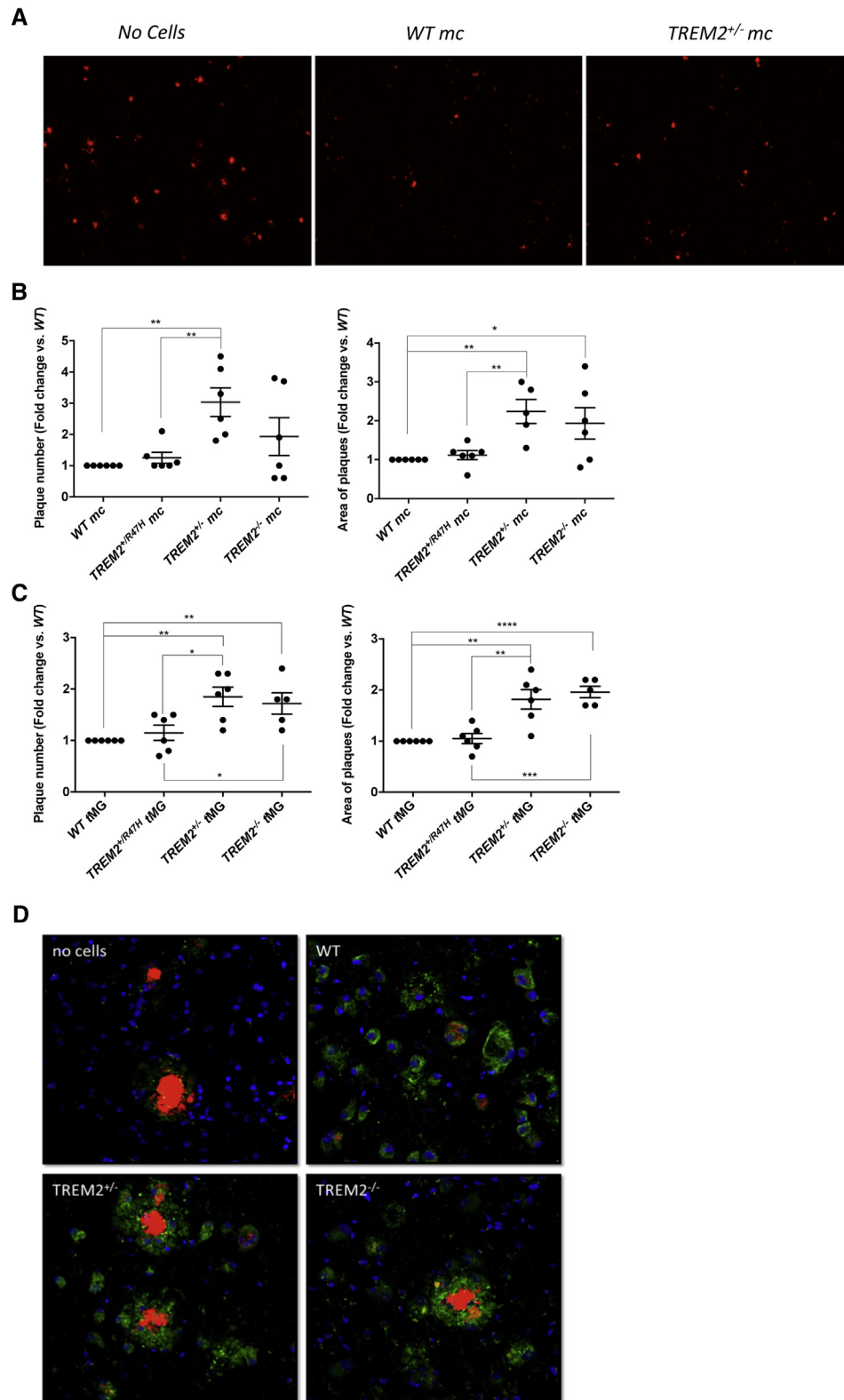
Fig. 5. *Ex vivo* amyloid plaque clearance by *TREM2 WT, TREM2$^{+/R47H}$, TREM2$^{+/-}$*, and *TREM2$^{-/-}$* mc, and tMG. (A) *TREM2 WT* monocytes (mc) versus *TREM2$^{+/-}$* mc compared to control (no cells) were cultured for 24 h on *APP/PS1$^{+/-}$* cryosections, which were then stained with thiazine red to visualize the amyloid plaques. (B, C) Quantification of amyloid plaque numbers and area based on thiazine red staining after incubation of brain cryosections with (B) mc (24 h) or (C) tMG (16 h); for each cell line, two independent differentiations were performed to derive mc and tMG. Each dot within the same cell line represents data obtained from a different brain cryosection; three to four images of cortical areas were acquired on the Zeiss Axio Imager A2 for each cryosection; data

as the optimal time point for analysis (Supplementary Fig. 4B). However, when tMGs were plated on the cryosections for 24 h, most plaques were cleared (Supplementary Fig. 4C). Therefore, we assessed plaque clearance by tMGs 16 h after plating (Supplementary Fig. 4C) and clearance by hPSC monocytes 24 h after plating on cryosections (Fig. 5A).

We observed a significant decrease in plaque removal by $TREM2^{+/-}$ monocytes and tMGs compared with WT cells at 24 h and 16 h, respectively (Fig. 5A, B, C). Similar results were obtained for $TREM2^{-/-}$ tMGs (Fig. 5C). Although the difference between the number of plaques for WT and $TREM2^{-/-}$ monocytes was not significantly different due to interexperimental variability (Fig. 5B), the persistent plaque area was significantly increased for $TREM2^{-/-}$ compared with WT monocytes (Fig. 5B). Confocal images illustrated amyloid plaque (thiazine red) removal by WT, $TREM2^{+/-}$, and $TREM2^{-/-}$ progeny ($LAMP1^+$, green, to identify lysosomes in monocytes and tMGs [46]) compared with slices without human cells (Fig. 5D). By contrast, $TREM2^{+/R47H}$ mutant monocytes and tMGs did not affect the number of plaques nor the total plaque size (Fig. 5B, C).

4. Discussion

As loss of TREM2 surface expression and the clinical $TREM2^{+/R47H}$ heterozygous mutation result in amyloid pathology [4–6], we here assessed if such mutant microglia might show reduced amyloid plaque clearance. We demonstrated, using a series of isogenic genome-edited hPSCs differentiated to monocytes and tMGs, that phagocytosis of both *E. coli* fragments and human amyloid plaques is significantly impaired for $TREM2^{+/-}$ and $TREM2^{-/-}$, but not $TREM2^{+/R47H}$ hPSC progeny.

First, we differentiated hPSCs to monocytes using the Yanagimachi protocol [35]. Magnetically isolated $CD14^+$ monocytes were then further transdifferentiated to tMGs using a combination of recombinant human M-CSF and IL34, as in Douvaras et al. (2017) [47]. Compared with PB monocytes, a set of microglial genes was significantly higher expressed in tMGs, with the exception of *CX3CR1*. This is in line with Douvaras et al. (2017) who suggested that expression of *CX3CR1* by microglia is seen chiefly early during microglial development. When we compared the normalized log1p CPM for *CX3CR1* of tMGs from our RNAseq study pooled with cultured fetal and adult human microglia, PB monocytes, and hPSC-induced microglia-like cells (RNAseq from Abud et al., 2017 [41]), *CX3CR1* was more highly expressed in PB monocytes compared with microglia (-like) samples.

Thus, under which circumstances *CX3CR1* is expressed should be further studied.

Comparison of tMGs with hPSC monocytes and PB monocytes somewhat surprisingly demonstrated that hPSC monocytes were quite similar to tMGs, whereas both differed significantly from PB monocytes. This was shown by qRT-PCR analysis for a set of microglial genes and confirmed based on the RNAseq studies from us and Abud et al. [41]. Thus, hPSC-tMGs resemble hPSC-microglia described in other studies, as well as cultured human microglia. However, so-called monocytes differentiated from hPSCs using the Yanagimachi protocol also resemble cultured microglia and much less PB monocytes. As culture of PB monocytes for 48 h in the hPSC-monocyte culture medium induced the expression of microglial genes, we hypothesize that this is due to the *in vitro* culture.

The best model to study the role of *TREM2* mutations would be human brain-derived microglia, which is difficult due to limited access to human brains. However, the ability to create microglia-like cells from hPSCs can now overcome this limitation. Therefore, we created a series of isogenic hPSCs by either knocking in the $TREM2^{+/R47H}$ mutation in one allele or knocking out one or both copies of *TREM2* ($TREM2^{+/-}$ and $TREM2^{-/-}$ hPSCs). These lines allow for the analysis of the effect of heterozygous or homozygous loss of *TREM2* as well as the role of the heterozygous R47H mutation on microglial function, and this is independent of possible genetic modifiers. Quantitative RT-PCR for *TREM2* transcripts demonstrated that *TREM2* transcripts were significantly decreased in $TREM2^{+/-}$ and even more in $TREM2^{-/-}$ hPSC monocytes and tMGs. Moreover, *TREM2* genome engineered lines were successfully differentiated to tMGs, based on the expression profile of a panel of microglial genes.

In agreement with current literature [29], we demonstrated decreased phagocytosis of pHrodo-linked *E. coli* fragments by $TREM2^{+/-}$ and $TREM2^{-/-}$ tMGs. We also found reduced amyloid plaque clearance by $TREM2^{+/-}$ and $TREM2^{-/-}$ tMGs. By contrast, Brownjohn et al. [33] found no phagocytic defect in *E. coli* uptake in microglia-like cells derived from TREM2 $T66M^{+/-}$, $T66M^{-/-}$ and $W50C^{-/-}$ hPSCs. One explanation for this discrepancy might be the use of different media (defined microglia medium containing IL34 and GM-CSF in Brownjohn et al. vs. minimal RPMI medium with no cytokines in our *E. coli* phagocytosis assay). Alternatively, differences in the mutations studied in Brownjohn et al. (T66M/W50C) and our study (heterozygous and homozygous knockout of *TREM2*) may be responsible for the discordant results. As the phagocytic impairment of $TREM2^{-/-}$ tMGs was not

represent means with SEM and *P* values by unpaired *t*-test; *$P \leq .05$; **$P < .005$; ***$P < .001$; ****$P < .0001$. (D) Confocal microscopy images of cortical thiazine red–stained amyloid plaques (red) and LAMP1-stained human mc (green) derived from *WT* versus $TREM2^{+/-}$ and $TREM2^{-/-}$ mc after 24 h of incubation on $APP/PS1^{+/-}$ cryosections (not representative for all cortical areas). No LAMP1 staining (green) was detected when no human cells were added. Abbreviations: tMG, transdifferentiated microglia-like cells; WT, wild-type.

more profound than that of $TREM2^{+/-}$ tMGs, we hypothesize that phagocytosis is directly affected once $TREM2$ mRNA expression is decreased at least 80% compared with WT tMGs.

Our data on the $TREM2^{+/R47H}$ tMGs are mostly in line with data from Kleinberger et al. [29] who used $R47H$ transduced HEK cells, also demonstrating no decrease in pHrodo-linked $E.\ coli$ uptake. However, although we did not observe reduced amyloid plaque clearance by $TREM2^{+/R47H}$ tMGs, the Kleinberger study found decreased uptake of amyloid β_{1-42} by $R47H$ transduced HEK cells. This may reflect differences between amyloid plaques and amyloid β_{1-42}, or the cell type studied.

To assess amyloid plaque clearance from cryosections, it was necessary to guide the hPSC monocytes and tMGs to the plaques with mAb11 because in the absence thereof, amyloid phagocytosis was barely detectable [32], and cryosections disintegrated after 3–4 days of co-culture. It is likely that without use of mAb11, microglia-like cells try to remove the necrotic nonviable tissue of the repeatedly frozen and thawed cryosected mouse brain, which interfered with the specific phagocytosis of amyloid plaques. The use of the mAb11 precluded assessment of a possible defect in migration caused by loss of $TREM2/TREM2^{+/R47H}$ cells. In addition, we cannot exclude some degree of opsonization contributing to the phagocytosis. However, the fact that both independent phagocytosis assays demonstrated impaired phagocytic capacity by $TREM2^{+/-}$ and $TREM2^{-/-}$ hPSC-derived tMGs supports our conclusion that only $TREM2^{+/-}$ and $TREM2^{-/-}$ directly impair phagocytosis. Future studies assessing plaque phagocytosis from cryosections or slice cultures of human brain tissue from AD patients co-cultured with $TREM2^{+/-}$ or $TREM2^{-/-}$ hPSC-derived tMG will be of interest for further confirmation of this phenotype.

In respect to the lack of a phagocytic phenotype for $TREM2^{+/R47H}$ tMGs, one should take into account that the biggest risk factor of AD, aging, is not recreated in tMGs derived from hPSCs. One could consider generating tMGs by direct transdifferentiation of fibroblasts from elderly patients with LOAD with a $TREM2^{+/R47H}$ mutation that may retain such an "aged signature" (as shown by Mertens et al., 2015 [48] for transdifferentiated neurons), once such protocols become available. Alternatively, $TREM2^{+/R47H}$ tMGs could be allowed to age by grafting in immune-compromised and microglia-depleted AD or SAMP8 mice and then reanalyzed or exposed to different ligands. Transcriptome analysis of such samples might reveal functions affected by this mutation upon aging.

Finally, transcriptome analysis revealed that loss of $TREM2$ is associated with a decreased expression of genes involved in extracellular matrix structure (integrin signaling) and transmembrane transporter activity, which suggests that loss of $TREM2$ may not only impair tMG-mediated phago-

cytosis but may in general affect the extent to which microglia can react/adapt to a changing microenvironment. $TREM2^{-/-}$ tMGs also expressed numerous genes involved in receptor-ligand activity, receptor-regulator activity, calcium ion binding, and cytokine activity more highly than WT tMGs, suggesting that $TREM2$ mutant tMGs might be proinflammatory (in agreement with the study by Hamerman et al. [21]). Future studies will be of interest to further uncover deranged integrin and cytokine/chemokine signaling in $TREM2^{-/-}$ tMGs.

To conclude, this is, to our knowledge, the first study using an $ex\ vivo$ amyloid plaque clearance assay, highly relevant to AD, to study the effect of $TREM2$ mutations in human microglia-like cells. We demonstrated that homozygous or heterozygous loss of $TREM2$, but not presence of the $TREM2^{+/R47H}$ mutation, directly impaired the ability of hPSC-derived monocytes and tMGs to phagocytose $E.\ coli$ and clear amyloid plaques, which might thus contribute to AD pathology. Future mechanistic studies on human $TREM2^{+/R47H}$ tMGs will be needed to determine why $TREM2^{+/R47H}$ is associated with a 3-fold increased risk for LOAD.

Supplementary data

Supplementary data to this article can be found online at https://doi.org/10.1016/j.jalz.2018.09.006.

RESEARCH IN CONTEXT

1. Systematic review: The authors reviewed the literature using PubMed. Current literature describes amyloid pathology for homozygous *T66M TREM2* carriers and a 3-fold increased risk for late-onset Alzheimer's disease for heterozygous *R47H* carriers. There have been several publications on the effect of *TREM2* mutations on cell function. Relevant citations are appropriately cited.

2. Interpretation: Our findings demonstrate for the first time that heterozygous presence of the *TREM2 R47H* mutation does not affect amyloid plaque clearance of hPSC-derived microglia-like cells, shown to resemble human primary microglia, and is solely disrupted upon heterozygous or homozygous loss of *TREM2*. During finalization of their manuscript, Brownjohn et al. published the derivation of other *TREM2* mutant hPSC microglia, which they incorporated in their manuscript.

3. Future directions: The manuscript proposes more studies on aged human $TREM2^{+/R47H}$ microglia-like cells to further unravel why it poses the highest risk factor of late-onset Alzheimer's disease.

References

[1] Hardy JA, Higgins GA. Alzheimer's disease: the amyloid cascade hypothesis. Science 1992;256:184–5.

[2] Goate A, Goate A, Chartier-Harlin M-C, Chartier-Harlin MC, Mullan M, Mullan M, et al. Segregation of a missense mutation in the amyloid precursor protein gene with familial Alzheimer's disease. Nature 1991;349:704–6.

[3] Tanzi RE. The genetics of Alzheimer disease. Cold Spring Harb Perspect Med 2012;2. a006296–6.

[4] Guerreiro R, Wojtas A, Bras J, Carrasquillo M, Rogaeva E, Majounie E, et al. TREM2 variants in Alzheimer's disease. N Engl J Med 2013;368:117–27.

[5] Jonsson T, Stefansson H, Steinberg S, Jonsdottir I, Jonsson PV, Snaedal J, et al. Variant of TREM2 associated with the risk of Alzheimer's disease. N Engl J Med 2013;368:107–16.

[6] Ghezzi L, Carandini T, Arighi A, Fenoglio C, Arcaro M, De Riz M, et al. Evidence of CNS β-amyloid deposition in Nasu-Hakola disease due to theTREM2Q33X mutation. Neurology 2017;89:2503–5.

[7] Guerreiro R, Hardy J. Genetics of Alzheimer's disease. Neurotherapeutics 2014;11:732–7.

[8] Rosenthal SL, Kamboh MI. Late-onset alzheimer's disease genes and the potentially implicated pathways. Curr Genet Med Rep 2014; 2:85–101.

[9] Nasu T, Tsukahara Y, Terayama K. A lipid metabolic disease-"membranous lipodystrophy-"an autopsy case demonstrating numerous peculiar membrane-structures composed of compound lipid in bone and bone marrow and various adipose tissues. Acta Pathol Jpn 1973;23:539–58.

[10] Hakola HP. Neuropsychiatric and genetic aspects of a new hereditary disease characterized by progressive dementia and lipomembranous polycystic osteodysplasia. Acta Psychiatr Scand Suppl 1972; 232:1–173.

[11] Mosher KI, Wyss-Coray T. Microglial dysfunction in brain aging and Alzheimer's disease. Biochem Pharmacol 2014;88:594–604.

[12] De Strooper B, Karran E. The Cellular Phase of Alzheimer's Disease. Cell 2016;164:603–15.

[13] Akiyama H. Inflammatory response in Alzheimer's disease. Tohoku J Exp Med 1994;174:295–303.

[14] Sessa G, Podini P, Mariani M, Meroni A, Spreafico R, Sinigaglia F, et al. Distribution and signaling of TREM2/DAP12, the receptor system mutated in human polycystic lipomembraneous osteodysplasia with sclerosing leukoencephalopathy dementia. Eur J Neurosci 2004;20:2617–28.

[15] Varnum MM, Clayton KA, Yoshii-Kitahara A, Yonemoto G, Koro L, Ikezu S, et al. A split-luciferase complementation, real-time reporting assay enables monitoring of the disease-associated transmembrane protein TREM2 in live cells. J Biol Chem 2017;292:10651–63.

[16] Colonna M. TREMs in the immune system and beyond. Nat Rev Immunol 2003;3:445–53.

[17] Colonna M, Wang Y. TREM2 variants: new keys to decipher Alzheimer disease pathogenesis. Nat Rev Neurosci 2016;17:201–7.

[18] Cuyvers E, Bettens K, Philtjens S, Van Langenhove T, Gijselinck I, van der Zee J, et al. Investigating the role of rare heterozygous TREM2 variants in Alzheimer's disease and frontotemporal dementia. Neurobiol Aging 2014;35:726. e11–9.

[19] Corder EH, Saunders AM, Strittmatter WJ, Schmechel DE, Gaskell PC, Small GW, et al. Gene dose of apolipoprotein E type 4 allele and the risk of Alzheimer's disease in late onset families. Science 1993;261:921–3.

[20] Krasemann S, Madore C, Cialic R, Baufeld C, Calcagno N, Fatimy El R, et al. The TREM2-APOE Pathway Drives the Transcriptional Phenotype of Dysfunctional Microglia in Neurodegenerative Diseases. Immunity 2017;47:566–9.

[21] Hamerman JA, Jarjoura JR, Humphrey MB, Nakamura MC, Seaman WE, Lanier LL. Cutting edge: inhibition of TLR and FcR responses in macrophages by triggering receptor expressed on myeloid cells (TREM)-2 and DAP12. J Immunol 2006;177:2051–5.

[22] Jay TR, Hirsch AM, Broihier ML, Miller CM, Neilson LE, Ransohoff RM, et al. Disease progression-dependent effects of TREM2 deficiency in a mouse model of Alzheimer's disease. J Neurosci 2017;37:637–47.

[23] Yuan P, Condello C, Keene CD, Wang Y, Bird TD, Paul SM, et al. TREM2 haplodeficiency in mice and humans impairs the microglia barrier function leading to decreased amyloid compaction and severe axonal dystrophy. Neuron 2016;90:724–39.

[24] Ulrich JD, Finn M, Wang Y, Shen A, Mahan TE, Jiang H, et al. Altered microglial response to Aβ plaques in APPPS1-21 mice heterozygous for TREM2. Mol Neurodegener 2014;9:20.

[25] Wang Y, Cella M, Mallinson K, Ulrich JD, Young KL, Robinette ML, et al. TREM2 lipid sensing sustains the microglial response in an alzheimer's disease model. Cell 2015;160:1061–71.

[26] Ulland TK, Song WM, Huang SC-C, Ulrich JD, Sergushichev A, Beatty WL, et al. TREM2 maintains microglial metabolic fitness in Alzheimer's disease. Cell 2017;170:649–663.e13.

[27] Song WM, Joshita S, Zhou Y, Ulland TK, Gilfillan S, Colonna M. Humanized TREM2 mice reveal microglia-intrinsic and -extrinsic effects of R47H polymorphism. J Exp Med 2018;215:745–50.

[28] Mazaheri F, Snaidero N, Kleinberger G, Madore C, Daria A, Werner G, et al. TREM2 deficiency impairs chemotaxis and microglial responses to neuronal injury. EMBO Rep 2017;18:1186–98.

[29] Kleinberger G, Yamanishi Y, Suárez-Calvet M, Czirr E, Lohmann E, Cuyvers E, et al. TREM2 mutations implicated in neurodegeneration impair cell surface transport and phagocytosis. Sci Translational Med 2014;6. 243ra86–6.

[30] Takahashi K, Rochford CDP, Neumann H. Clearance of apoptotic neurons without inflammation by microglial triggering receptor expressed on myeloid cells-2. J Exp Med 2005;201:647–57.

[31] N'Diaye E-N, Branda CS, Branda SS, Nevarez L, Colonna M, Lowell C, et al. TREM-2 (triggering receptor expressed on myeloid cells 2) is a phagocytic receptor for bacteria. J Cell Biol 2009; 184:215–23.

[32] Xiang X, Werner G, Bohrmann B, Liesz A, Mazaheri F, Capell A, et al. TREM2 deficiency reduces the efficacy of immunotherapeutic amyloid clearance. EMBO Mol Med 2016;8:992–1004.

[33] Brownjohn PW, Smith J, Solanki R, Lohmann E, Houlden H, Hardy J, et al. Functional Studies of Missense TREM2 Mutations in Human Stem Cell-Derived Microglia. Stem Cell Reports 2018;10:1–28.

[34] Yin J, Liu X, He Q, Zhou L, Yuan Z, Zhao S. Vps35-dependent recycling of Trem2 regulates microglial function. Traffic 2016; 17:1286–96.

[35] Yanagimachi MD, Niwa A, Tanaka T, Honda-Ozaki F, Nishimoto S, Murata Y, et al. Robust and highly-efficient differentiation of functional monocytic cells from human pluripotent stem cells under serum- and feeder cell-free conditions. PLoS One 2013;8:e59243.

[36] Muffat J, Li Y, Yuan B, Mitalipova M, Omer A, Corcoran S, et al. Efficient derivation of microglia-like cells from human pluripotent stem cells. Nat Med 2016;22:1358–67.

[37] Funk WD, Labat I, Sampathkumar J, Gourraud P-A, Oksenberg JR, Rosler E, et al. Evaluating the genomic and sequence integrity of human ES cell lines; comparison to normal genomes. Stem Cell Res 2012;8:154–64.

[38] Bard F, Cannon C, Barbour R, Burke R-L, Games D, Grajeda H, et al. Peripherally administered antibodies against amyloid β-peptide enter the central nervous system and reduce pathology in a mouse model of Alzheimer disease. Nat Med 2000;6:916–9.

[39] Radde R, Bolmont T, Kaeser SA, Coomaraswamy J, Lindau D, Stoltze L, et al. Aβ42-driven cerebral amyloidosis in transgenic mice reveals early and robust pathology. EMBO Rep 2006;7:940–6.

[40] Kuhn P-H, Wang H, Dislich B, Colombo A, Zeitschel U, Ellwart JW, et al. ADAM10 is the physiologically relevant, constitutive alphasecretase of the amyloid precursor protein in primary neurons. EMBO J 2010;29:3020–32.

[41] Abud EM, Ramirez RN, Martinez ES, Healy LM, Nguyen CHH, Newman SA, et al. iPSC-Derived human microglia-like cells to study neurological diseases. Neuron 2017;94:278–9.

[42] Yusa K, Rad R, Takeda J, Bradley A. Generation of transgene-free induced pluripotent mouse stem cells by the piggyBac transposon. Nat Methods 2009;6:363–9.

[43] Shen B, Zhang W, Zhang J, Zhou J, Wang J, Chen L, et al. Efficient genome modification by CRISPR-Cas9 nickase with minimal off-target effects. Nat Methods 2014;11:399–402.

[44] Bohrmann B, Baumann K, Benz J, Gerber F, Huber W, Knoflach F, et al. Gantenerumab: a novel human anti-Aβ antibody demonstrates sustained cerebral amyloid-β binding and elicits cell-mediated removal of human amyloid-β. J Alzheimers Dis 2012;28:49–69.

[45] Delrieu J, Ousset PJ, Vellas B. Gantenerumab for the treatment of Alzheimer's disease. Expert Opin Biol Ther 2012;12:1077–86.

[46] Barrachina M, Maes T, Buesa C, Ferrer I. Lysosome-associated membrane protein 1 (LAMP-1) in Alzheimer's disease. Neuropathol Appl Neurobiol 2006;32:505–16.

[47] Douvaras P, Sun B, Wang M, Kruglikov I, Lallos G, Zimmer M, et al. Directed differentiation of human pluripotent stem cells to Microglia. Stem Cell Reports 2017;8:1516–24.

[48] Mertens J, Paquola ACM, Ku M, Hatch E, Böhnke L, Ladjevardi S, et al. Directly reprogrammed human neurons retain aging-associated transcriptomic signatures and reveal age-related nucleocytoplasmic defects. Cell Stem Cell 2015;17:705–18.